Dynamic Performance of Vibration Absorbers for Low-Frequency Vibration Isolation Systems

Shamsul Bashir [*1, 2, b] and Nasim Akhtar[1, 2, c]

[1]Academy of Scientific and Innovative Research (AcSIR), Ghaziabad-201002, India

[2]CSIR-Central Road Research Institute, New Delhi-110025, India

[*]Corresponding author, Email: shamsulbashir123@gmail.com and shamsulbashir.crri@nic.in

[b]Ph. D Research Scholar

[c]Sr. Principal Scientist

Email: crri.nasim@gmail.com and nasim.crri@nic.in

Abstract

This paper introduces a novel mass-spring system utilizing a well-designed polyurethane pad vibration isolator, conceptually designed as a floating slab track structure. The floating slab track is considered one of the most efficient countermeasures for attenuating the vibration impacts of underground high-speed railways. The dynamic performance of the polyurethane slab track structure was studied and compared with the steel-spring floating slab track using a conventional mathematical approach based on the principle of influence lines. The study investigates vibration isolation performance under dynamic vehicle loads at speeds ranging from 180 to 300 kmph. Results indicate a significant reduction in slab dynamic responses with increasing speed. Both systems demonstrate excellent vibration-damping ability, with the steel mass-spring system being approximately 18% more efficient in vibration reduction than the polyurethane mass-spring system.

Keywords: Deflection, stiffness, natural frequency, vibration attenuation, stress, fatigue

Introduction

Ground-borne vibrations generated by underground high-speed railways (HSR) are becoming more significant. This is attributed to a decrease in human resistance to vibration, an increase in the utilization of equipment sensitive to vibrations, and the aging of existing structures[1]. In most countries, HSR networks are expanding rapidly, and conventional lines are being upgraded to higher speeds. India is also constructing its first HSR corridor, with several other HSR projects in the planning stage. Thus, the ground vibrations generated by HSR are expected to remain a major topic for researchers and designers worldwide. To understand the generation mechanisms, develop modeling techniques, and implement vibration control measures, extensive research has been conducted in this field. Advanced theoretical and computational approaches have been established globally[2,3] because predicting ground vibration is crucial for identifying generation mechanisms, recognizing crucial attributes, synthesizing measured data, and developing mitigation measures. Various methodologies have been extensively studied to minimize structural vibrations. The observation and mitigation of structural vibrations have been ongoing for 50 years. In 1972, Yao[4] was the first to introduce advanced mitigation theory into civil engineering, initiating subsequent investigations into structural vibration isolation.

HSR has specific attributes, constraining its use to higher speeds, heavy load distribution, and the laying of track structures on bridges, tunnels, and other situations. The high-magnitude vibrations caused by HSR can be monitored at various stages throughout the direction of wave propagation from the source to the receiver end[5,6]. In most cases, the most practicable means of vibration mitigation is at the source, which is the track structure itself, achieved by modifying track characteristics and/or incorporating elastic bearings into the track[7-10]. One of the most vital vibration mitigation measures adopted at the source is the use of ballastless slab tracks with very low stiffness, commonly utilized in HSR corridors[7]. In this

study, we consider one such ballastless slab structure, namely the floating slab track (FST). FSTs are generally designed using two important damping materials, namely steel springs (SS) and rubber/polyurethane (PU) pads[1,2,11-13]. With a sequence of SS isolators and PU pads, these FSTs support the second-stage concrete, also known as the floating slab (FS), of the track structures. Therefore, an FS and the SS/PU vibration shock absorber constitute the primary components of the system. The system, however, is not self-contained because it is connected to the fasteners, the base concrete (tunnel base) wall, or the top of the bridge structure[14].

Vibration mitigation against ground-borne vibration follows the same fundamentals as that against earthquakes[15]. However, depending on the seismic energy forces, which, in the case of ground-borne energy forces, are numerous degrees of magnitude lesser in intensity and have a wider and greater frequency response, both the governing principle and the effective application vary in context[16]. The Single Degree of Freedom (SDOF) model, which depicts the slab structure as a stiffer weight held on some type of spring or isolation bearing, backed by a stiffer concrete foundation, is frequently used to explain the fundamentals of vibration dissipation. The basic principle is to make the natural frequency of the system on its foundation as far below the excitation frequency as possible. The proportion of the deflection magnitude of the slab mass to the levied ground movement at the foundation provides a description of the vibration mitigation at the origin. The accurate representation explaining the frequency response of this proportion varies based on the attenuation model utilized. However, the important components are similar across all contexts. Vibration dampers act to magnify each low-frequency vibration, particularly high at the natural frequency of the system. These dampers are only efficient for frequency bands greater than 1.414 times the isolation frequency, beyond which the mitigation accelerates with frequency, and damping of the system helps to restrict the resonant frequency[17]. A conventional approach to improving

mitigation performance at lower frequencies is to further decrease the system's natural frequency by reducing stiffness or increasing mass.

The need to precisely monitor the efficiency of vibration mitigation techniques before their implementation has recently increased the significance of vibration modeling and simulation for underground HSR's. The performance of these vibration mitigation measures has been observed in various theoretical and empirical research works on different types of slab track structures [18–23]. This paper specifically concentrates on the effectiveness of two types of FST systems, namely the steel spring FST (SSFST) and discrete polyurethane FST (PUFST), for controlling ground-borne vibrations in underground HSR. Modeling has been conducted using a conventional mathematical approach based on the principle of influence line diagrams, which considers dynamic amplification factors when evaluating the system's dynamic responses[24]. The vibration mitigation efficiencies of both developed systems were evaluated and compared.

Assessment of vibration isolation of MSS

In this section, the equations of motion for the vehicle-slab track system are solved for a vertical axle load using the concept of influence lines. The slab track is assumed to have a cross slope (θ) of 0° with a longitudinal gradient (δ_{long}) of 2%. Therefore, the slab track's pitch (β) is calculated as 0.11 employing Equation (1).

$$\beta = \left(\arctan\left(\delta_{long}\right)\right).\frac{180}{\pi} \quad (1)$$

The more general case of low-frequency SSFST and PUFST has been evaluated by incorporating low-stiffness SS and PU pad isolators under the second-stage concrete slab. Figures 1*(a)* and 1(*b)* show the cross-sections of tunnel-SSFST and tunnel-PUFST, respectively. The equivalent depths of the FST, considering the second moment of area $\left(d_{eq.I}\right)$ and modulus of rigidity $\left(d_{eq.EI}\right)$, are evaluated as Equations (2) and (3), respectively.

$$d_{eq.I} = \left(12\left(\frac{I_{Y.FST}}{b}\right)\right)^{\frac{1}{3}} \quad (2)$$

$$d_{eq.EI} = \left(12\left(\frac{EI_{Y.FST}}{E_{Conc.}b}\right)\right)^{\frac{1}{3}} \quad (3)$$

The research is a continuation of the previously published work by the authors, and, therefore, the same methodology has been adopted[25]. However, some of the crucial formulations are summarized below.

For the SDOF system, the fundamental natural frequency due to mass gravity can be given by Equation (4)[26].

$$f_n = 5/\left(\frac{d_s}{10}\right)^{1/2} \quad (4)$$

$$d_s = F/k \quad (5)$$

where, d_s is the static deflection in mm, and Equation (5) is the basic formula for its calculation, with F representing the loading and k being the stiffness of the vibration attenuation system.

For dynamic systems where precision in the analysis becomes very important, the following equation (Equation (6)) can be used to determine the system's natural frequency.

$$f_n = 5/\left[\left(\frac{\left(\frac{\left(d_{D_{Out}} + d_{D_{In}}\right)}{2}\right).\mu_t + d_{S_V}}{10}\right)\right]^{1/2} \quad (6)$$

where d_{S_V}, $d_{D_{Out}}$, and $d_{D_{In}}$ represent the vertical static and dynamic deflections at the wheel's external and internal surfaces, respectively. μ_t is the mass of the train.

The transmissibility factor for the vibration attenuation system can be given as Equation (7)[27].

$$T = \sqrt{\frac{1 + 4\xi^2\eta^2}{(1-\eta^2)^2 + 4\xi^2\eta^2}} \quad (7)$$

Where, η and ξ are the tuning and damping ratios of the spring-mass system, respectively.

The transmissibility function (T) gives the vibration attenuation ability (VdB) and the degree of isolation (I) of the spring-mass systems. The relationships between T and VdB, and T and I are given by Equation (8) and Equation (9), respectively[27].

$$VdB = -20logT \quad (8)$$

$$I\% = (1 - T).100 \quad (9)$$

Basic aspects of performing dynamic analysis

Vehicle and FST parameters

A vehicle with a maximum design speed of 320 kmph and an axle load $(F_{V_{axle}})$ of 170 kN has been adopted[28]. The unsprung train mass (the part of the train mass oscillating at the same degree of freedom as the track slab) has been considered to be 15%. The length, height, and width of the wagon are 18.7 m, 4.1 m, and 2.89 m, respectively. The axle spacing in the same bogie is 3 m. The slab track comprises two UIC60 rails with a modulus of elasticity of $2.1x10^{11}$ N/m² and a mass per linear rail meter of the rail of 60.34 kg/m for each rail. The fasteners have vertical and horizontal stiffness of 60 and 100 kN/mm, respectively. The mass per linear meter of fasteners (μ_{FAST}) is 92.3 kg/m. The longitudinal distance between rail fastenings is 0.67 m, and the FST panels have a maximum length of 30 meters. The concrete slab has a density (ρ_c) of 2400 kg/m^3 and a modulus of elasticity (E) of 30800 N/mm^2. Figure 1 shows the cross-sectional details of the FST systems used in the study.

Vibration isolator specifications

The design specifications of the SS isolator and PU pad isolator are provided in Tables 1 and 2, respectively.

The spring isolator consists of two springs, namely an external spring and an internal spring, each with two diameter springs. The vertical stiffness of the adopted SS isolator unit

has been taken as 5867 N/mm, and the damping ratio as 8%. According to code DIN EN 13906-1:2013-1[29], the permissible dynamic deflection amplitude for the adopted spring model in the external spring should be 7.715 mm, and for the internal spring, it should be 13.005 mm.

The PU isolator has a thickness of 40 mm and is composed of closed-cellular material. The vertical stiffness of the PU isolator unit has been taken as 24410 N/mm, and the damping ratio as 12%. According to code DIN 45673-7[30], the horizontal stiffness of the PU pad shall be considered at about 35% of the vertical stiffness, and maximum horizontal deformation shall be taken at about 70% of the material thickness.

The longitudinal spacing between the spring isolators was adjusted along with the speed of the train.

Evaluation of dynamic responses due to train load and FST system interaction

The study employs a traditional mathematical methodology to evaluate the dynamic and static responses induced by the dynamic interaction of the train and the FST systems. The FST is a massive spring-mass system composed of a concrete mass (FS) floating on a springy body (SS or PU pad isolators), as shown in Figures 1*(a)* and 1*(b)*. All calculations for the dynamic analysis of the spring-mass systems were performed by adopting the reference (25)[25]. For the fatigue verification of the SS isolator, the allowable spring stress, i.e., τ_k, should a maximum of 708.90 N/mm^2 in the external spring and 803.51 N/mm^2 in the internal spring, as specified in the Goodman diagrams in DIN EN 13906-1:2013-1[29]. However, for the fatigue strength verification of the PU isolator, the elastomers should be continuously strained at most 10 to 15% in compression[30,31]. This criterion determines the maximum load capacity of a given isolator. Therefore, for verifying the fatigue strength of the PU isolator, the threshold value of the load on the PU isolator in the horizontal and vertical directions was considered to be 15%.

To explore the vehicle speed's impact on PUFST and evaluate and differentiate the differences in the dynamic responses and, subsequently, the vibration absorption between the PUFST and SSFST (presented in ref. 25), the vehicle speed was varied from 180 to 300 kmph.

Impact of vehicle speed on static and dynamic deflection attributes of slab track structures

Figures 2 and 3 depict the deflection of the SSFST and PUFST systems, respectively, on the external and internal sides of the track as the speed of the train increases. In Figures 2*(a)* and 2*(b)*, and Figures 2*(c)* and 2*(d)*, dynamic deflections are represented on the external and internal sides of the FST systems for speeds ranging from 180 to 300 kmph.

As the difference is not visible in these graphs, delta values have been calculated for speeds ranging from 200 to 300 kmph, relative to a speed of 180 kmph. Figures 3*(a)* and 3*(b)* depict static and dynamic deflections on the internal and external sides of the slab track systems at 180 kmph. Figures 3*(c)* and 3*(d)*, as well as Figures 3*(e)* and 3*(f)*, present delta-valued deflection graphs externally and internally of slab track systems at speeds ranging from 200 to 300 kmph.

The train's speed appears to have a significant impact on both the static and dynamic responses of the FST systems. However, the deflection results for both the SSFST and PUFST systems remain within acceptable limits.

The figures show that the optimum dynamic deflection at the wheel's external side, $d_{D_{Out}}$ and internal side, $d_{D_{In}}$, for SSFST, reduces from 4.37 to 4.17 mm and 3.22 to 2.72 mm, respectively, as the train velocity increases from 180 to 300 kmph. However, the optimum dynamic horizontal deflection, d_{D_H}, used to calculate the system's natural frequency rises from 0.33 to 0.41 mm. The static deflection of the SSFST externally ($d_{S_{Out}}$) and internally ($d_{S_{In}}$) reduces from 9.64 to 8.62 mm.

Similarly, for the PUFST, the optimum dynamic deflection at the external, $d_{D_{Out}}$ of the wheel increases from 1.69 to 1.70 mm, and at the internal of the wheel reduces from 1.24 to 1.11 mm, respectively. The optimum dynamic horizontal deflection, d_{D_H}, to determine the system's natural frequency rises from 0.66 to 0.87 mm. The static deflection of the PUFST externally ($d_{S_{Out}}$) and internally ($d_{S_{In}}$) reduces from 3.14 to 2.98 mm.

Impact of vehicle speed on the longitudinal spacing between the vibration isolators

As the speed of the train increases, the longitudinal spacing, S_L, between the vibration isolators decreases. However, the spacing between the SS isolators in SSFST was found to be less than that between the PU isolators in PUFST. For the SSFST, the longitudinal spacing between the SS isolators decreases from 1220 to 1090 mm, and for the PUFST, the longitudinal spacing between the PU isolators decreases from 1650 to 1570 mm, for an increase in speed from 180 to 300 kmph. The reason for the decrease in spacing is that as the train speed increases, more dynamic forces are generated on the slab track, necessitating the use of additional isolators to dissipate the vibrational energy.

Impact of vehicle speed on cumulative vertical loading of the slab track structures

The influence of train velocity on the cumulative vertical load is shown in Figure 4*(a)*, in which the subsequent vertical load on both the slab track systems at the external of the wheel, $F_{R_V Out}$, rises from 98.42 to 103.63 kN, and the subsequent vertical load on the internal of the wheel, $F_{R_V In}$, reduces from 71.58 to 66.37 kN. The similar trend is followed because the mass of the slabs is constant for both slab tracks.

Impact of vehicle speed on vibration mitigation of the slab track structures

Figures 4*(b)* and 4*(c)* illustrate how an increase in vehicle speed influences the vertical stiffness and, consequently, the vibration dissipation capacity of the system. As the vehicle speed rises, the stiffness of the SSFST and PUFST also rises, reducing the system's

vibration-damping potential. However, slab track systems have a high vibration dissipation capacity.

The spectral assessment has been conducted in 1/3-octave frequency bands to determine the insertion loss utilizing the natural frequency and damping ratio of the spring-mass systems, The distinctive graphs for the correlation between the 1/3-octave frequency bandwidths varying from 0.8 to 630 Hz, and the velocity of the train, are shown in Figure 5. From the figure, it can be observed how the vibration-attenuating potential of the FST systems varies with the rise in speed. To express vibration levels more implicitly and to find out the absolute impact of vibrations on the human body and sensitive structures, the global/total vibration level (GVL) measurement was calculated using Equation (10).

$$GVL = 10log\left(10^{\frac{VL_1}{10}} + 10^{\frac{VL_2}{10}} + 10^{\frac{VL_3}{10}} \ldots + 10^{\frac{VL_n}{10}}\right) \quad 10$$

where, VL_1, VL_2, VL_3,..,VL_n are the vibration emissions at different frequency bands in the overall frequency spectrum.

Therefore, Figure 6 depicts GVL attenuation graphs for the correlation between the natural frequency and the optimum vibration dissipation of spring-mass systems. It is indicated from the figure that the vertical spring rate of SSFST, k_{VFST}, rises from 9.62 to 10.77 kN/mm/m as the train speed increases, thus lowering the vibration isolation effectiveness of the system from 30.7 to 29.5 VdB.

Figures 6*(a)*, 6*(c)*, and 6*(e)* depict the optimal vibration dissipation in relation to the natural frequency of vibration of the SSFST system. As the train speed rises from 180 to 300 kmph, the natural frequency of the SSFST system, f_{V_n}, rises from 4.95 to 5.23 Hz, lowering the system's vibration isolation potential. The GVL absorption, on the other hand, rises as the natural frequency falls. At speeds of 300, 280, 250, 220, 200, and 180 kmph, the optimum absorption of the vibration is 29.5, 29.7, 30, 30.2, 30.5, and 30.7 VdB for natural frequencies of 5.23, 5.19, 5.13, 5.07, 5.01, and 4.95 Hz, respectively.

The similar trend as in SSFST was followed in PUFST. However, for the PUFST, the vertical spring rate, k_{VFST} increases from 29.59 to 31.10 kN/mm/m, thus lowering the vibration isolation potential of the system from 26 to 24.8 VdB, respectively. Figures 6*(b)*, 6*(d)*, and 6*(f)* show the optimum reduction of the vibration concerning the natural frequency of vibration of the PUFST system. As the train speed rises from 180 to 300 kmph, the natural frequency of the slab track system, f_{V_n}, rises from 8.63 to 8.85 Hz, lowering the system's vibration-damping potential. The GVL absorption, on the other hand, rises as the natural frequency falls. At speeds of 300, 280, 250, 220, 200, and 180 kmph, the GVL absorption is 24.8, 25, 25.3, 25.5, 25.8, and 26 VdB for natural frequencies of 8.85, 8.82, 8.76, 8.74, 8.68, and 8.63 Hz, respectively.

Fatigue verification calculations

As mentioned above, when vibrant forces are applied to a SS isolator and a PU pad isolator, the allowable stresses produced in the SSFST must not supersede the stress array specified in the Goodman diagrams[29]. For the PUFST, the stress range should be such that the maximum loading should not exceed 15% of the total load[30,31.]

For a speed of 180 kmph, the allowable stresses in the external and internal springs of a spring unit on the outside and inside of the SSFST are shown in Figures 7*(a)* and 7*(b)*. Similarly, Figures 7*(c)* and 7*(d)* depict the allowable stresses in the external and internal springs of a spring unit on the outside and inside of the SSFST for a speed of 300 kmph, respectively.

All of the Goodman diagrams were matched to DIN EN 13906-1:2013-11[29], Figure (11). All the graphs have followed a similar pattern to the allowable stress graphs. Table 3 shows the stresses induced in the SS isolators with speed for fatigue verification of SSFST. With a rise in vehicle speed from 180 to 300 kmph, the maximum dynamic stress in the outer spring of the SS isolator outside the track reduces from 540.74 to 521.35 N/mm^2, and inside

the track, it decreases from 487.66 to 448.04 N/mm^2. Similarly, for the inner spring of the SS isolator, the maximum value of dynamic stress outside the slab track reduces from 487.66 to 448.04 N/mm^2, and the maximum dynamic stress on the inside of the slab track reduces from 545.90 to 448.04 N/mm^2.

Figures 8*(a)* and 8*(b)* show the fatigue verification (PU loading diagram) in the vertical and horizontal directions on the PUFST for speeds of 180 and 300 kmph, respectively. The vertical loading on the PU increases from 14.8% to 15% up to a speed of 250 kmph and then shows a slight decrease up to 300 kmph. Similarly, horizontal loading increases from 10.2% to 10.7% with the rise in the train speed from 180 to 250 kmph and then shows a slight decrease of 0.1% at both speeds of 280 and 300 kmph. However, in all cases, it remains under the permissible limit of 15%, as shown in Table 4. The slight decrease in loading percentage for higher speeds occurred due to the decrease in the deflection of PU. The reason could be that when the speed is increased, the requisite deflection of the pad isolator to absorb excitation energy is reduced.

The above discussion indicates that, according to the mentioned codes and rules, the maximum dynamic stress in the SS isolator falls within the permissible limit. Additionally, the vertical and horizontal loading on the PU pad remains within the threshold values. Consequently, the SS isolator and PU pad used in the investigation exhibit efficient fatigue strength and extended lifespan. They can effectively withstand cyclic loading, thereby enhancing the serviceability and durability of the track structure.

Conclusions

The study focuses on the dynamic analysis of SSFST and PUFST, evaluating their vibration isolation effectiveness in HSR using a conventional mathematical approach and highlighting the differences between the two. The following conclusions can be drawn.

- With increasing train speed, the maximum vertical dynamic deflection of the SSFST reduces, while there is a slight increase in the deflection of the PUFST system.
- The longitudinal spacing between vibration isolators decreases as the train speed increases. For SSFST, the spacing between SS isolators in SSFST decreased from 1220 to 1090 mm, and for PUFST, the spacing between PU isolators decreased from 1650 to 1570 mm as the speed increased from 180 to 300 kmph.
- The stiffness of both SSFST and PUFST increases with the increase in vehicle speed, leading to an increase in natural frequency and a decrease in the vibration isolation effectiveness of the slab track systems.
- SSFST outperforms PUFST in frequency reduction and vibration attenuation. The frequency of SSFST was established at 5.23 Hz for a speed of 300 kmph, resulting in an overall vibration dissipation of up to 29.5 VdB. In contrast, for the same speed, the frequency of PUFST was established at 8.85 Hz, resulting in an overall vibration dissipation of up to 24.8 VdB.
- SS and PU pad isolators have good durability and serviceability, making them efficient and successful for HSR systems.

Declaration of conflicting interests

The authors declare no potential conflicts of interest concerning the research, authorship, and/or publication of this article.

Acknowledgment

The authors express gratitude to the Director, CSIR- Central Road Research Institute, New Delhi, and the Academy of Scientific and Innovative Research, Ghaziabad, for kindly permitting the publication of this paper. Additionally, the authors thank the CSIR-Human Resource Development Group for awarding the Senior Research Fellowship to Ms. Shamsul Bashir facilitating the completion of this research.

References

1. Lei, X. and Jiang, C. Analysis of vibration reduction effect of steel spring floating slab track with finite element. Journal of Vibration and Control, 2014, pp. 1–10, DOI: 10.1177/1077546314539372.
2. Xin, T. and Gao, L. Reducing slab track vibration into bridge using elastic materials in high speed railway. Journal of Sound and Vibration, 2011, vol. 330, pp. 2237–2248. doe: 10.1016/j.jsv.2010.11.023.
3. Lombaert, G., Degrande, G., François, S. and Thompson, D. J. Ground-borne vibration due to railway traffic: a review of excitation mechanisms, prediction methods and mitigation measures. Noise And Vibration Mitigation for Rail Transportation Systems, Springer, Berlin, Heidelberg, 2015, vol. 126, pp. 253-287.
4. Yao, T. P. Concept of structural control. Journal of the Structural Division, ASCE, 1972, vol. 98, issue 7, pp. 1567-1574.
5. Schillemans, L. Impact of sound and vibration of the north-south high-speed railway connection through the city of Antwerp, Belgium. Journal of Sound and Vibration, 2003, vol. 267, pp. 637–649.
6. Talbot J. P. Base-isolated buildings: towards performance-based design. Proceedings of the Institution of Civil Engineers, Structures and Buildings, 2016, vol. 169, issue SB8, pp. 574-582. http://dx.doi.org/10.1680/jstbu.15.00057.
7. Cox, S. J. and Wang, A. Effect of track stiffness on vibration levels in railway tunnels. Journal of Sound and Vibration, 2003, vol. 267, issue 3, pp. 565-573. https://doi.org/10.1016/S0022-460X(03)00724-7.
8. Vogiatzis, K. and Mouzakis, H. Ground-Borne Noise and Vibration Transmitted from Subway Networks to Multi-Storey Reinforced Concrete Buildings. Transport, 2018, vol. 33, issue 2, pp. 446-453. https://doi.org/10.3846/16484142.2017.1347895.

9. Carels, P. Low vibration & noise track systems with tunable properties for modern metro track construction. Metro's Impact on Urban Living, Proceedings of 2002 World Metro Symposium, Taipei, Taiwan, 2002, pp. 208-217, Taipei City Government.
10. Wagner, H. G. Attenuation of transmission of vibration and ground-borne noise by means of steel spring supported low-tuned floating trackbeds, Metro's Impact on Urban Living, Proceedings of 2002 World Metro Symposium, Taipei, Taiwan, 2002, pp. 223-228, Taipei City Government.
11. Rajaram, S. and Nelson, J. T. High-Performance Floating Slab Track: Design and Construction improvements Based on Lessons Learned from Prototype Slabs. National Academy of Sciences: Transportation Research Board, Journal of Transportation Research Board, 2019, vol. 2673, issue 1, pp. 300–309. DOI: 10.1177/0361198118823004.
12. Chowdhary, A. R. and Akhtar, N. (2021). Study of steel mass spring system with varying speeds in a tunnel. Current Science, 2021, vol. 121, no. 11. Doi: 10.18520/cs/v121/i11/1441-1451.
13. Forrest, J. A. and Hunt, H. E. M. Ground vibration generated by trains in underground tunnels. Journal of Sound and Vibration, 2006, vol. 294, issues 4-5, pp. 706–736. https://doi.org/10.1016/j.jsv.2005.12.031.
14. Yin, X. J., Huang, J. F., Gao, X. L., Wang, J. L. and Zhang, B. C. The application of steel spring floating slab track on vibration control and noise reduction in elevated tracks. Proceedings of the 4th International Symposium on Environmental Vibrations: Prediction, Monitoring, Mitigation and Evaluation, Beijing, China, 2009, 28–30 October, pp. 683–693.

15. Puguh, B. P. Analysis and Evaluation of Railway Track Systems on Soft Soil: Trackbed Thickness Design and Dynamic Track-Soil Interaction. Technische Universität München, 2017, pp. 1-298.
16. Naeim, F. and Kelly, J. M. Design of Seismic Isolated Structures: From Theory to Practice. Wiley, New York, NY, USA, 1999.
17. Shengyang, Z., Jizhong, Y., Chengbiao, C., et al. Application of dynamic vibration absorbers in designing a vibration isolation track at low-frequency domain. Proceedings of the Institution of Mechanical Engineers, Part F: Journal of Rail and Rapid Transit, 2017, vol. 231, issue 5, pp. 546–557. https://doi.org/10.1177%2F0954409716671549.
18. Crockett, A. R. and Pyke, J. R. Viaduct design for minimization of direct and structure-radiated train noise. Journal of Sound and Vibration, 2000, vol. 231, pp. 883–897.
19. Cui, F. and Chew, C. H. The effectiveness of floating slab track system—Part 1. Receptance methods. Applied Acoustics,2000, vol. 61, pp. 441–453.
20. Saurenman, H. and Phillips, J. In-service tests of the effectiveness of vibration control measures on the BART rail transit system. Journal of Sound and Vibration, 2006 vol. 293, pp. 888–900.
21. Hussein, M. F. M. and Hunt, H. E. M. An insertion loss model for evaluating the performance of floating-slab track for underground railway tunnels. 10th International Congress on Sound and Vibration, ICSV1, Stockholm, Sweden, 2003, 7–10 July.
22. Kuo, C. M., Huang, C. H. and Chen, Y. Y. Vibration characteristics of floating slab track. Journal of Sound and Vibration, 2008, vol. 317, pp. 1017–1034.

23. Lombaert, G., Degrande, G., Vanhauwere, B., Vandeborght, B. and Francois, S. The control of ground-borne vibrations from railway traffic by means of continuous floating slabs. Journal of Sound and Vibration, 2006, vol. 297, pp. 946–961.
24. Talbot, J. P. Base-isolated buildings: towards performance-based design. Proceedings of the Institution of Civil Engineers (Structures and Buildings), 2016, vol. 169, issue SB8, pp. 574–582. http://dx.doi.org/10.1680/jstbu.15.00057.
25. Bashir, S. and Akhtar, N. Development of Low-Frequency Mass Spring System for Underground High-Speed Railways. Journal of Vibration Engineering & Technologies, 2021, pp. 1-21. https://doi.org/10.1007/s42417-021-00392-w.
26. Bert, C. W. Relationship Between Fundamental Natural Frequency and Maximum Static Deflection for Various Linear Vibratory Systems. Journal of Sound and Vibration, 1993, vol. 162, issue 3, pp. 54-557. https://doi.org/10.1006/jsvi.1993.1139.
27. Paz, M. and Young, K. H. Structural Dynamics: Theory and Computation. Sixth Edition. Springer Nature Switzerland AG 2019, 2019. https://doi.org/10.1007/978-3-319-94743-3.
28. Connolly, D. P., Kouroussis, G., Woodward, P. K., et al. Field testing and analysis of high speed rail vibrations. Soil Dynamics and Earthquake Engineering, 2014, vol. 67, pp. 102–118. https://doi.org/10.1016/j.soildyn.2014.08.013.
29. DIN EN 13906-1:2013-11, Cylindrical Helical Springs made from Round Wire and Bar-Calculation and Design-Part 1: Compression Springs. German version EN 13906-1:2013 (German Title: Zylindrische Schraubenfedern aus runden Drähten und Stäben - Berechnung und Konstruktion - Teil 1: Druckfedern; Deutsche Fassung EN 13906-1:2013), 2013, pp. 1-39.
30. DIN 45673-7. Mechanical vibration - Resilient elements used in railway tracks - Part 7: Laboratory test procedures for resilient elements of floating slab track systems

(German Title: Mechanische Schwingungen - Elastische Elemente des Oberbaus von Schienenfahrwegen - Teil 7: Labor-Prüfverfahren für elastische Elemente von Masse-Feder-Systemen), 2010, pp. 1-22.

31. Introduction. Mechanical vibration and shock are present in varying degrees in virtually all locations where equipment and people function. The adverse effect of these disturbances can range from negligible to catastrophic depending on the severity of the disturbance and the sensitivity of the equipment, pp. 51-65. https://hutchinsonai.com/wp-content/uploads/2020/01/IsolatorsSelection.pdf.
32. ISO 1856:2018(E), Flexible cellular polymeric materials — Determination of compression set (German Title: Matériaux polymères alvéolaires souples — Détermination de la déformation rémanente après compression), pp. 1-4.
33. ISO 527-3:2018(E), Plastics — Determination of tensile properties — Part 3: Test conditions for films and sheets (German Title: Plastiques — Détermination des propriétés en traction — Partie 3: Conditions d'essai pour films et feuilles), pp. 1-7.
34. ISO 3302-1:2014(E), Rubber — Tolerances for products — Part 1: Dimensional tolerances (German Title: Caoutchouc — Tolérances pour produits — Partie 1: Tolérances dimensionnelles), pp. 1-10.
35. DIN 53513: 1990, Determination of the viscoelastic properties of elastomers on exposure to forced vibration at non-resonant frequencies, pp. 1-8.
36. DIN EN ISO 11925-2. Reaction to fire tests - Ignitability of products subjected to direct impingement of flame - Part 2: Single-flame source test (ISO 11925-2:2020); German version EN ISO 11925-2:2020 (German Title: Prüfungen zum Brandverhalten - Entzündbarkeit von Produkten bei direkter Flammeneinwirkung - Teil 2: Einzelflammentest (ISO 11925-2:2020); Deutsche Fassung EN ISO 11925-2:2020), 2020, pp. 1-39.

Table 1. Design specifications of SS-isolator[25,29]

Material Properties	**Values**	
Vertical stiffness, $k_{SS.V}$ (N/mm)	5867	
Horizontal stiffness, $k_{SS.H}$ (N/mm)	3688	
Damping ratio, ξ_{SS}	8 %	
	External Spring	**Internal Spring**
External diameter, D (mm)	132	60
Internal diameter, d (mm)	44	20
Number of turns (n)	3.5	7.5
Block height, L_c (mm)	206.8	174
Permissible dynamic deflection amplitude, $d_{DPerm.}$ (mm)	7.715	13.005
Shear Modulus, G (N/mm^2)	78500	
Modulus of Elasticity, E (N/mm^2)	206000	
Longitudinal spacing between the isolators, S_L (mm) – (speed decreasing)	1090-1220	

Table 2. Design specifications of PU-isolator[30, 32-36]

Material Properties	**Values**
Vertical stiffness, $k_{PU.V}$ (N/mm)	24410
Horizontal stiffness, $k_{PU.H}$ (N/mm)	2470
Damping ratio, ξ_{PU}	12 %
Material identification test	DIN 45673-7: 2010
Mechanical loss factor, n	0.05 to 1
Compression set in %	<5
Tensile stress at break in %	0.7 to 18
Elongation at break in %	400 to 500
Dimension check	Design thickness ± 2.5 mm for 40 mm Design thickness ± 1.6 mm for 25 mm Design thickness ± 1 mm for 12.5 mm
Modulus of Elasticity (Static), N/mm^2	0.7 to 200
Modulus of Elasticity (Dynamic), N/mm^2	0.9 to 350
Water absorption capacity (%)	Volume < 70 Mass < 300
Flammability	Class E
Longitudinal spacing between the isolators, S_L (mm) – (speed decreasing)	1570-1650

Table 3. Results for fatigue verification of SSFST

Speed (kmph)	**Vertical Deflection (mm)**	**Horizontal Deflection (mm)**	**Stress in external spring (N/mm^2)**		**Stress in internal spring (N/mm^2)**	
			Outside track	**Inside track**	**Outside track**	**Inside track**
180	16.83	2.17	540.74	487.66	545.90	490.10
200	16.66	2.16	535.86	477.20	540.92	479.25
220	16.52	2.17	532.14	465.60	537.10	467.14
250	16.42	2.18	529.60	459.25	534.46	460.48
280	16.20	2.18	523.27	451.62	528.02	452.68
300	16.12	2.18	521.35	448.04	526.03	448.95

Deflection is due to static and dynamic loading

Table 4. Results for fatigue verification of PUFST

Speed (kmph)	**Vertical Deflection (mm)**	**Horizontal Deflection (mm)**	**Vertical pad loading (%)**	**Horizontal pad loading (%)**
180	5.91	4.08	14.8	10.2
200	5.93	4.12	14.8	10.3
220	5.96	4.19	14.9	10.5
250	6.02	4.28	15	10.7
280	5.95	4.24	14.9	10.6
300	5.93	4.22	14.8	10.6

Deflection is due to static and dynamic loading

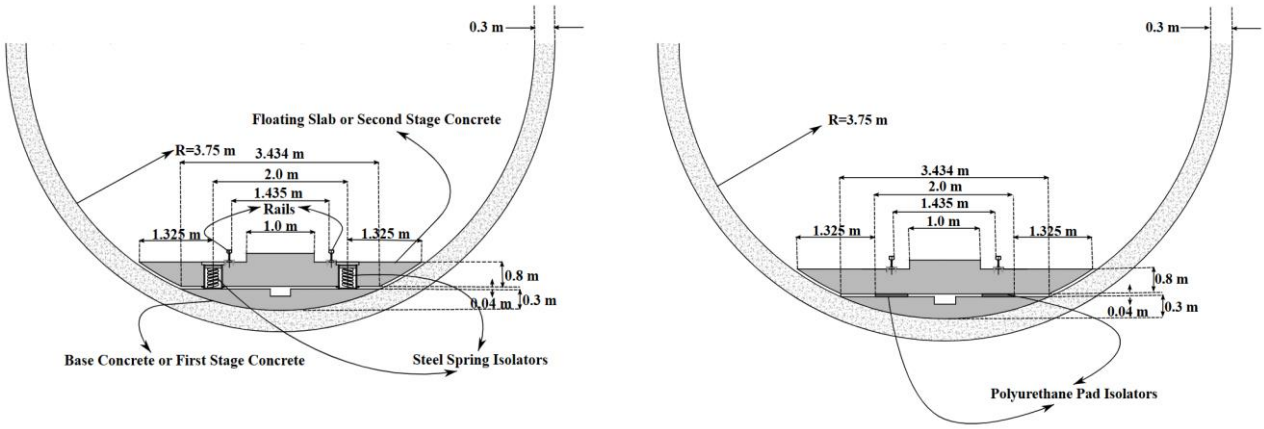

(a) ***(b)***

Figure 1. Cross-section of tunnel. ***(a)*** with SSFST and ***(b)*** with PUFST

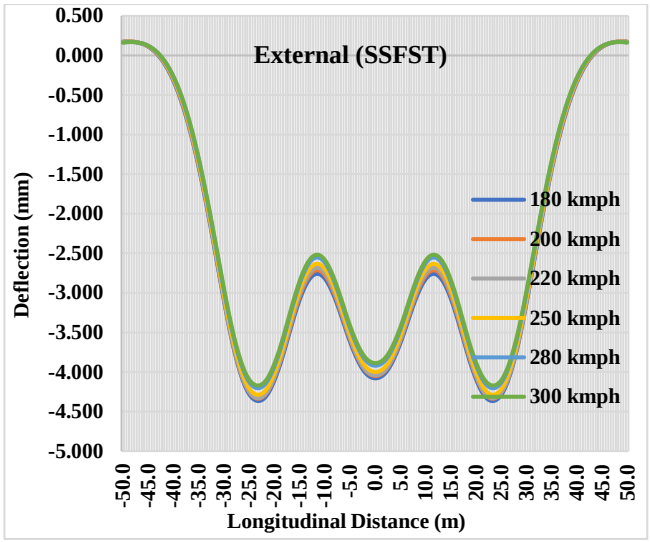

(a)

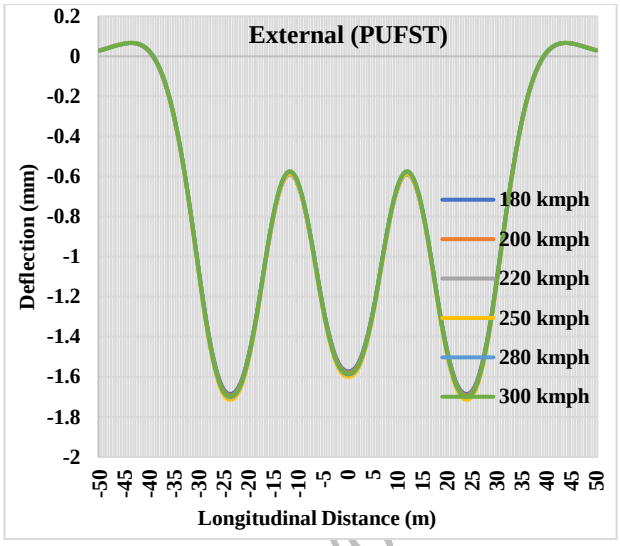

(b)

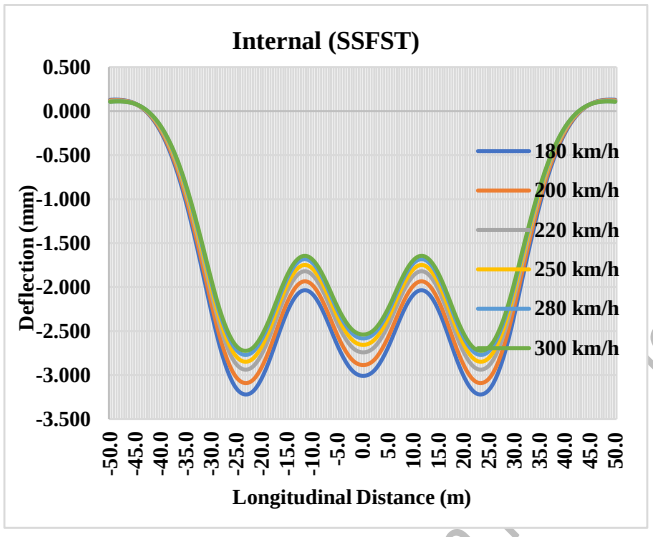

(c)

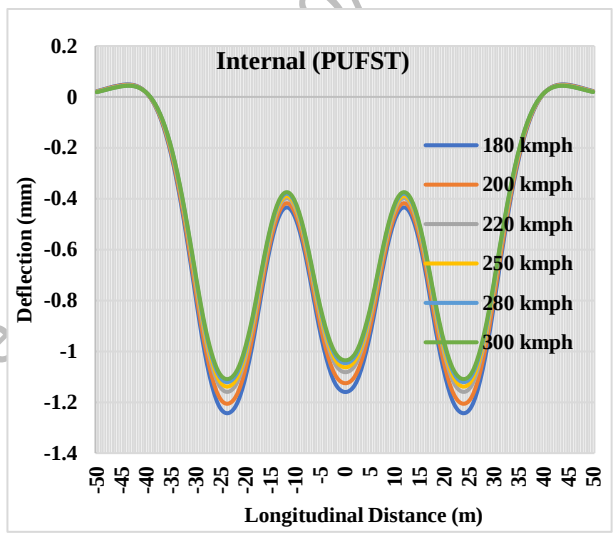

(d)

Figure 2. Dynamic deflections. ***(a, c)*** outside and inside of SSFST[25] and ***(b, d)*** outside and inside of PUFST

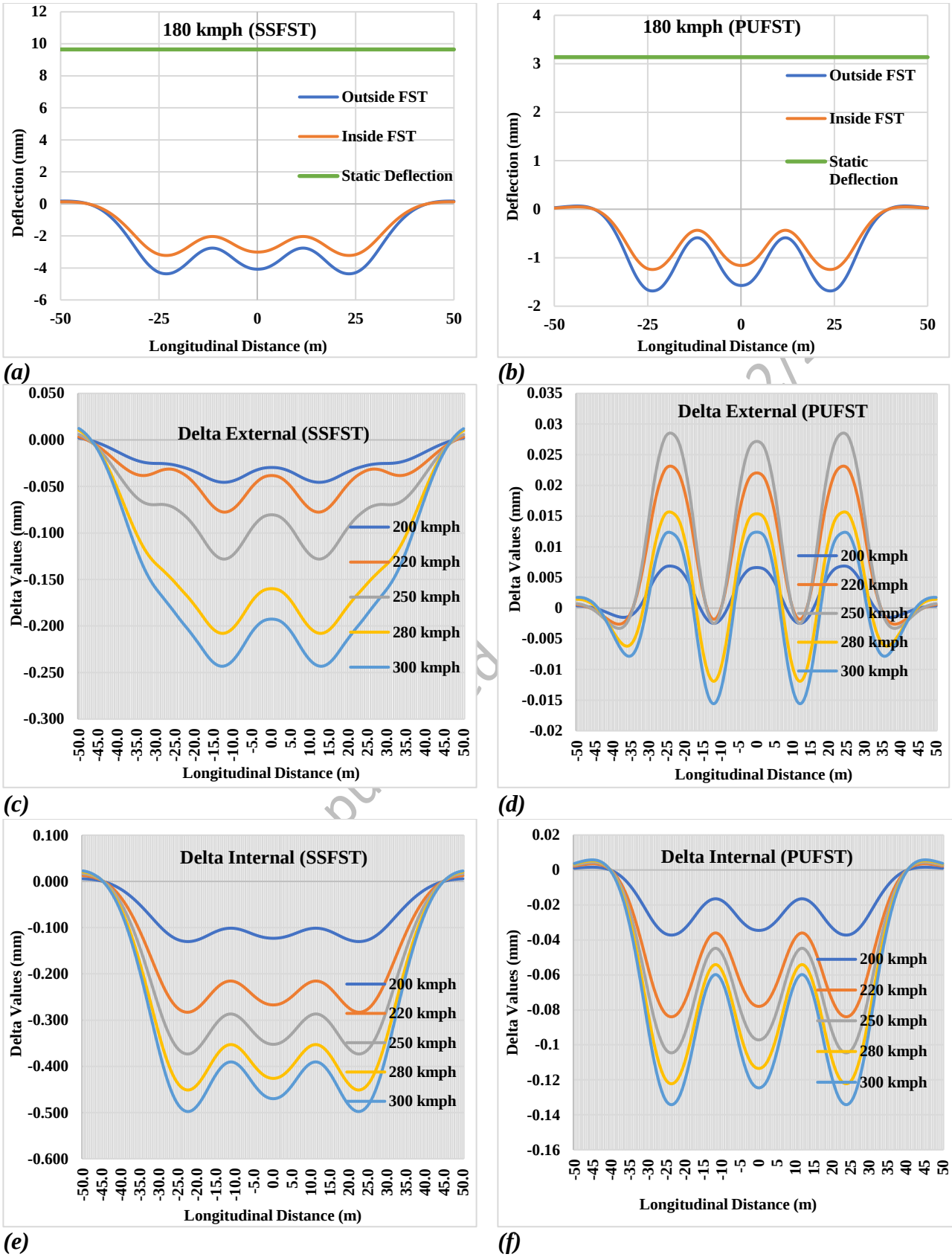

Figure 3. Deflection. ***(a, b)*** SSFST and PUFST at 180 kmph, ***(c, e)*** outside and inside of SSFST w.r.t Figure 3*a*[25], and ***(d, f)*** outside and inside of PUFST w.r.t Figure 3*b*

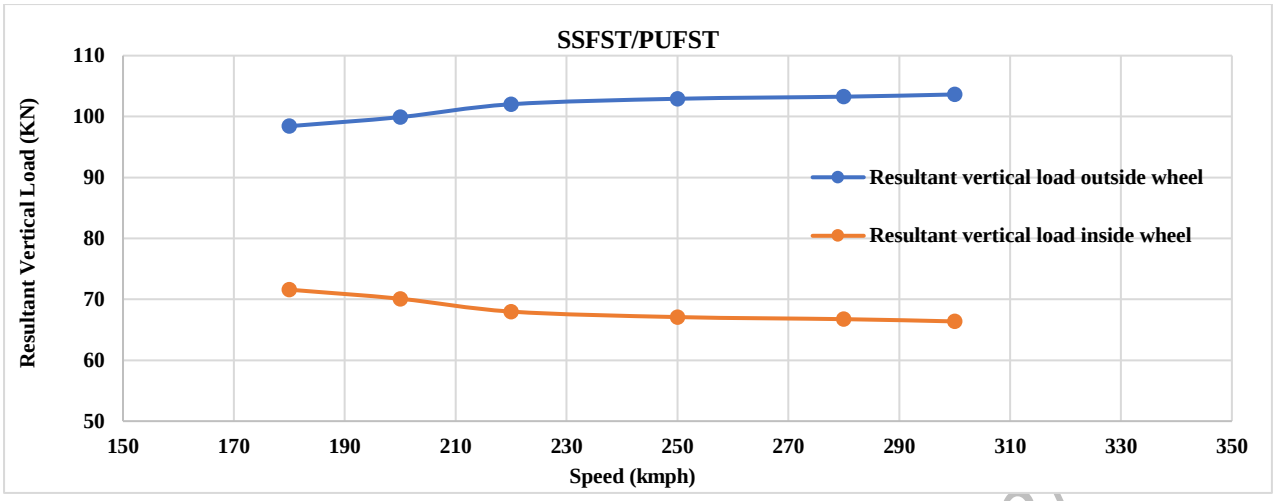

(a)

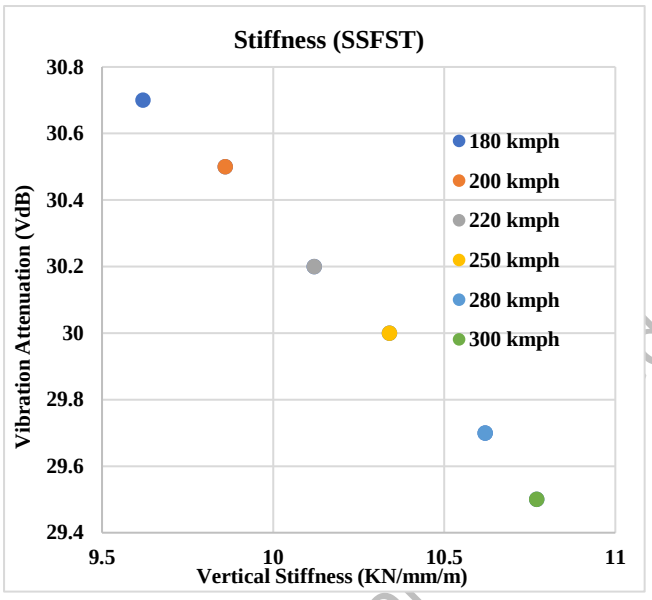

(b)

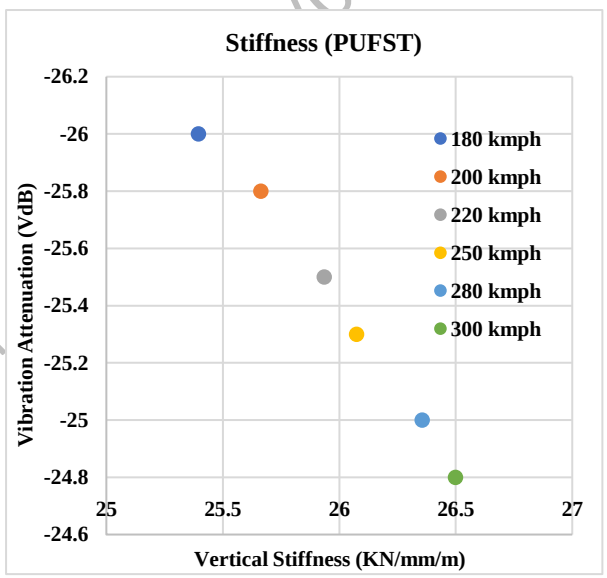

(c)

Figure 4. ***(a)*** Impact of speed on resultant vertical load on FST systems and ***(b, c)*** Impact of vertical stiffness on vibration attenuation of SSFST[25] and PUFST

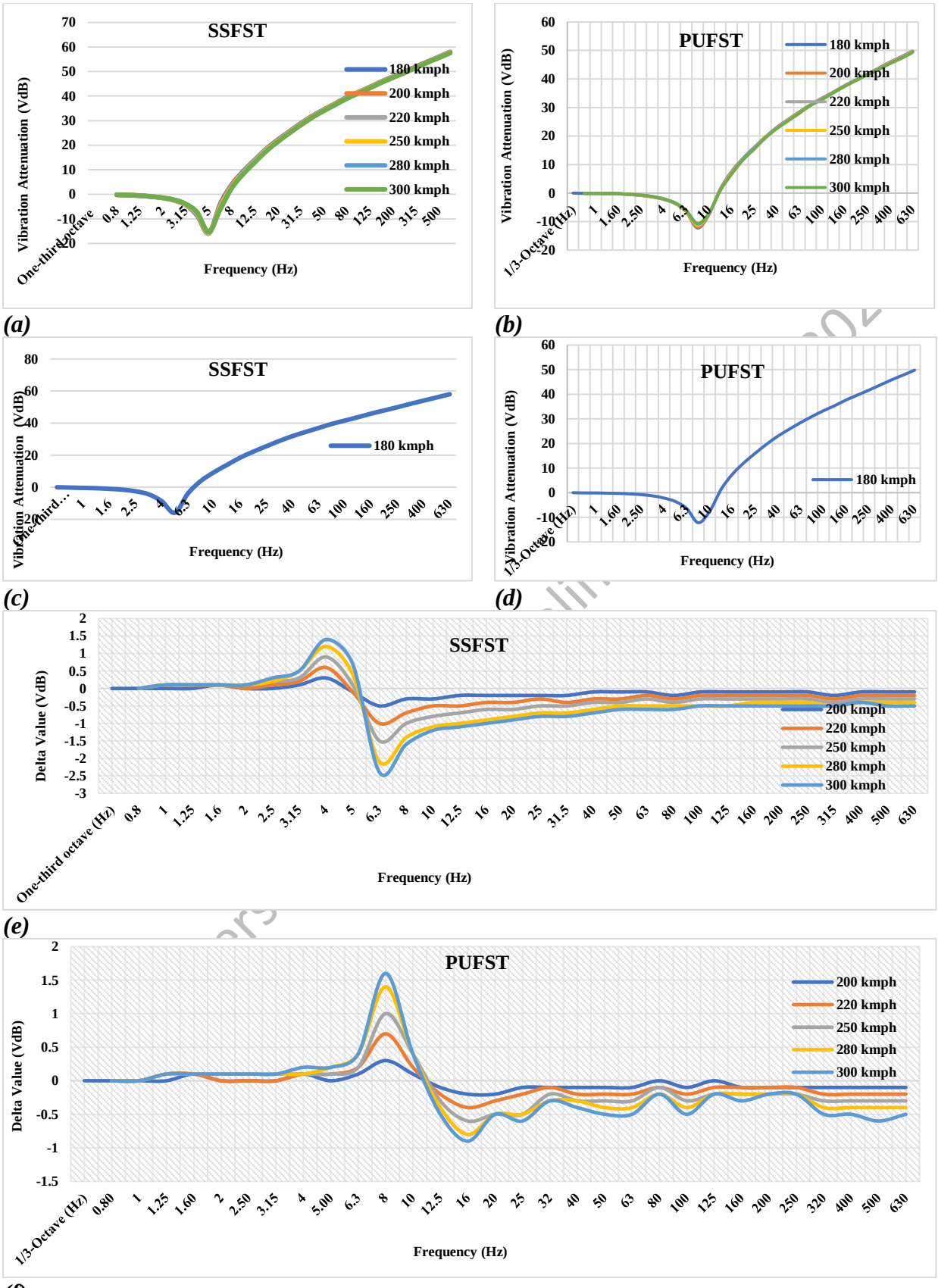

Figure 5. Attenuation and amplification by insertion loss (*VdB*) by SSFST and PUFST. ***(a. b)*** with speed increase, ***(c, d)*** at 180 kmph, and ***(e, f)*** SSFST[25] w.r.t Figure 5*c* and PUFST w.r.t Figure 5*d*

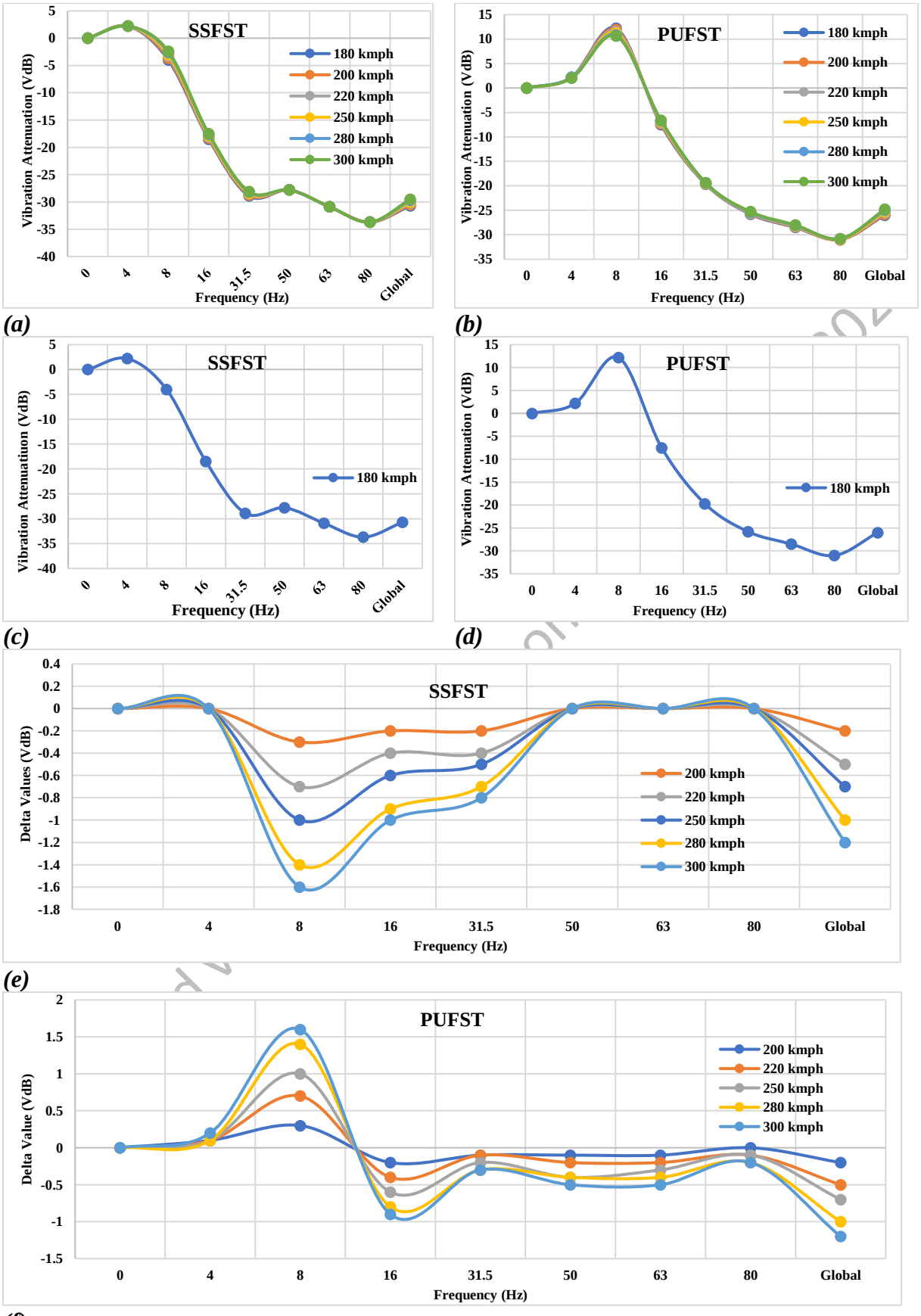

Figure 6. GVL attenuation (*VdB*) with SSFST[25] and PUFST. ***(a, b)*** speed increase, ***(c, d)*** at 180 kmph, and ***(e, f)*** SSFST[25] w.r.t Figure 6*c* and PUFST w.r.t Figure 6*d*

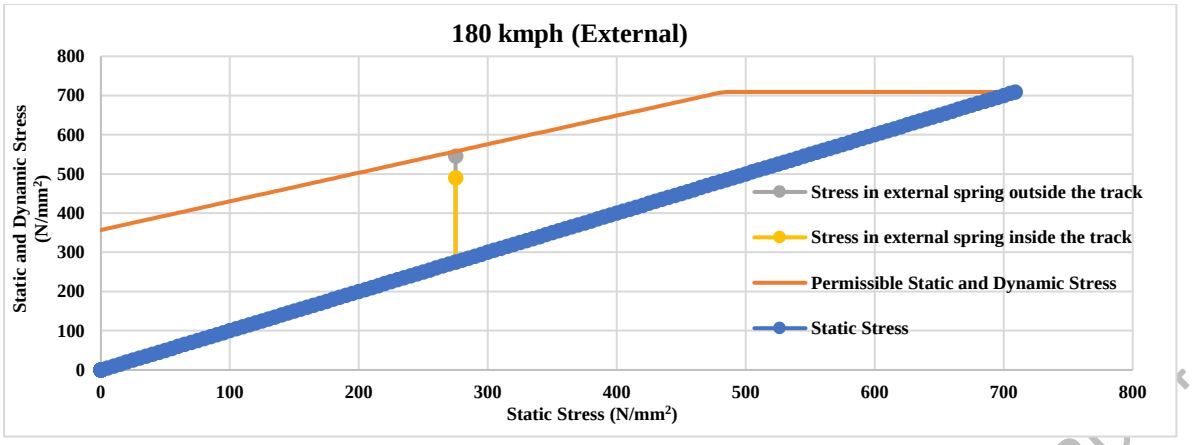

(a)

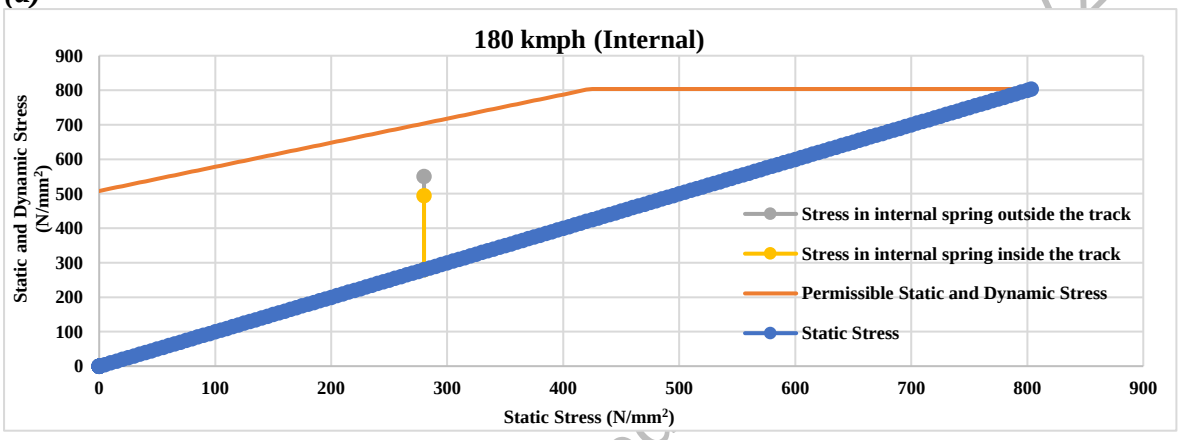

(b)

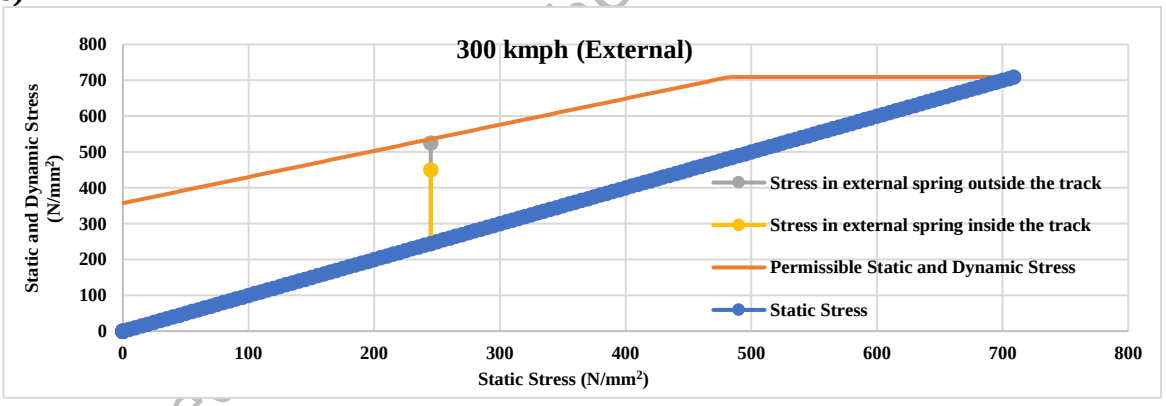

(c)

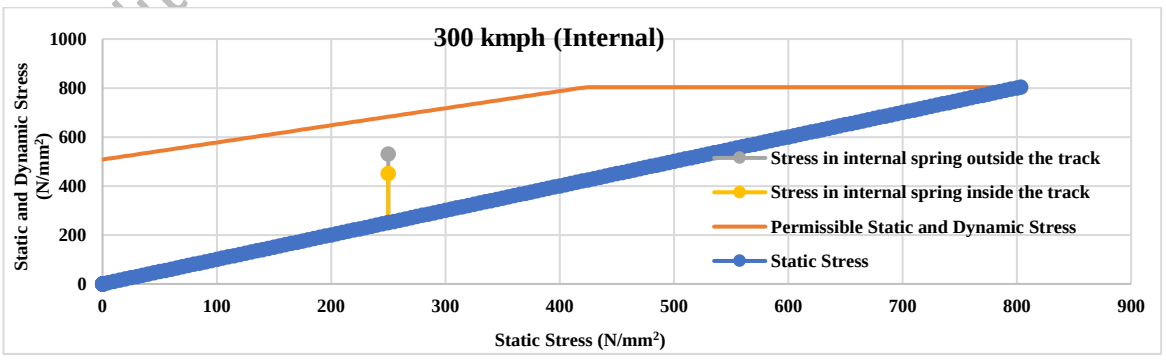

(d)

Figure 7. Allowable stresses in external and internal springs of SSFST for fatigue verification at ***(a, b)*** 180 kmph and ***(c, d)*** 300 kmph

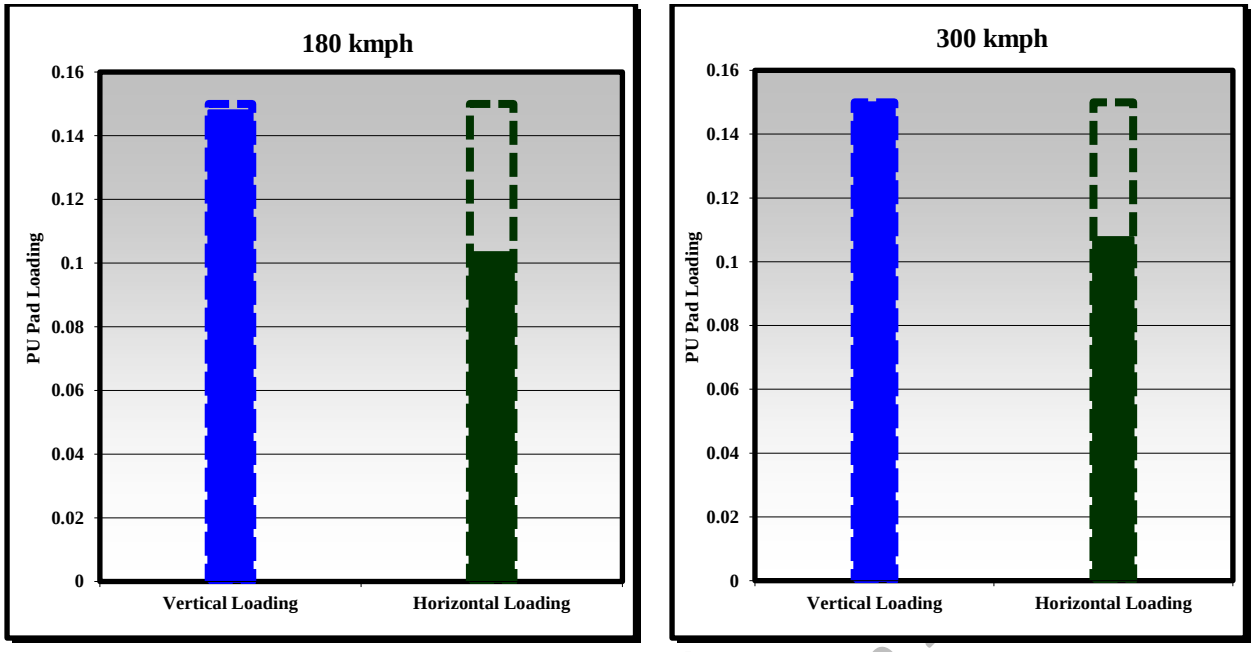

(a) ***(b)***

Figure 8. Pad loading diagram for fatigue verification at a speed of ***(a)*** 180 kmph and ***(b)*** 300 kmph